Investigating effects of local environment on bottlebrush conformations using super-resolution microscopy

Jonathan M. Chan, Avram C. Kordon, Muzhou Wang*

Department of Chemical and Biological Engineering, Northwestern University, Evanston, Illinois 60208, United States

Abstract

The single-chain physics of bottlebrush polymers plays a key role in their macroscopic properties. Although there has been effort in understanding the behavior of single isolated bottlebrushes, studies on their behavior in crowded, application-relevant environments have been insufficient due to limitations in characterization techniques. Here, we use single-molecule localization microscopy (SMLM) to study the conformations of individual bottlebrush polymers by direct imaging. Our previous work focused on bottlebrushes in a matrix of linear polymers, where our observations suggested their behavior was largely influenced by an entropic incompatibility between the bottlebrush side chains and the linear matrix. Instead, we focus here on systems where this effect is reduced: in solvent-swollen polymer materials and in systems entirely comprised of bottlebrushes. We measure chain conformations and rigidity using persistence length (l_p) as side chain molecular weight (M_{sc}) is varied. Compared to a system of linear polymers, we observe greater flexibility of the backbone in both systems. For bottlebrushes in bottlebrush matrices, we additionally observe a scaling relationship between l_p and M_{sc} that more closely follows theoretical predictions. For the more flexible chains in both systems, we reach the edge of our resolution limit and cannot visualize the entire contour of every chain. We comment on this limitation by discussing the aspect ratios of the features within the super-resolution images.

Introduction

The applications of bottlebrush polymers are widespread, ranging from electronics,[1,2] biomedical materials,[3–6] additive manufacturing,[7,8] and recyclable materials.[9] Often, these applications utilize bottlebrush polymers in crowded systems such as bulk materials or concentrated solutions, where the behavior of individual chains within a field of neighboring chains determines many of the resulting properties. For example, the soft mechanical properties of bottlebrush elastomers arise from their rigid conformations that result in decreased entanglements.[4] In another example, concentrated polymer solutions exhibit unique flow properties, such as low entanglements and strain hardening due to side chain interactions.[10–14] A deeper understanding of single-chain physics in crowded environments would enable better materials design for myriad applications.

In crowded environments, our knowledge of bottlebrush behavior has been limited. For dilute solutions, small-angle neutron scattering has revealed transitions between globule and rod-like geometries at different molecular architectural regimes and a concentration dependence of polymer size and rigidity.[10,15,16] However, these studies are often limited to conditions below the necessary concentrations for applications, such as inks for additive manufacturing.[7] In studying solid bottlebrush materials, scattering techniques have also revealed that backbones possess higher degrees of rigidity depending on their position within self-assembled structures of multiblock systems.[17,18] However, because scattering is indirect and requires model fitting, it is difficult to reveal details about single polymer chains. Helium ion microscopy is a powerful imaging tool that has been applied to bulk bottlebrush systems, and studies utilizing this method have revealed phenomena such as liquid crystal-like chain alignment in annealed samples. However, this surface-specific technique may not accurately characterize behavior within the bulk of a material.[19]

Instead, single-molecule localization microscopy (SMLM) has the ability to probe within crowded systems and shows great promise in studying single bottlebrushes to understand their single chain behavior.[20,21]

Previously, we have used SMLM to study bottlebrushes dispersed within a solid matrix composed of linear polymers.[22,23] These studies were insufficient for investigating bottlebrush conformations in the bulk, because the surrounding linear matrix introduced potential immiscibility effects with the side chains of the bottlebrush polymers. Studying a wider range of systems provides a deeper knowledge of bottlebrush behavior within other relevant environments. For example, many applications rely on solution-based casting methods, where the addition of solvent is likely to affect chain behavior. In many processes involving solution-based casting, materials transition from dilute to concentrated solution and then to the solid state, so studying behavior at these intermediate junctions is highly relevant to understanding their final morphology.[24,25] Additionally, bottlebrushes within a linear matrix insufficiently capture behavior within many applications, where materials are often entirely comprised of bottlebrush polymers.[6,26] There are numerous theoretical studies that dive into the question of chain behavior in bottlebrush melts,[27–29] but currently there is a deficit in experimental techniques to explore similar systems. Diversifying the systems studied by SMLM is attractive because there is interest in understanding their behavior in many other application-relevant environments.

In this work, we focus on the effects of changing the environments around bottlebrush polymers and compare these results to our previous studies in linear matrices. We first investigate bottlebrush conformations within linear matrices swollen by a good solvent. These solvent-swollen systems are analogous to concentrated polymer solutions. We also study the conformation of bottlebrush polymers within a bottlebrush matrix. Studying these systems significantly builds upon

our earlier work by reducing the immiscibility effects previously observed between linear and bottlebrush polymers. Furthermore, it expands the scope to more application-relevant systems that rely on bulk or crowded environments.

Methods and Materials

All materials were acquired from Sigma-Aldrich unless otherwise stated. Bottlebrush polymers were synthesized using previously published methods using a grafting-from approach.[30–32] Poly(hydroxyl-ethylmethacrylate) (Polymer Source M_n = 245.6 kg/mol, $Đ$ = 1.19) (PHEMA) was functionalized by coupling with α-bromoisobutyryl bromide to form poly(2-(2-bromoisobutyryloxy)ethyl methacrylate) (PBIEM). The dye-labeled species were synthesized and characterized in a past study.[23] Unlabeled bottlebrush polymers for the polymer matrices of melts were synthesized using the same method. Characterization of the side chain molecular weight of the matrix polymers was performed by gel permeation chromatography (GPC) using an Agilent 1260 Infinity II system equipped with two columns in series (PLgel MIXED-B LS, 7.5 x 300 mm, 10 μm) and a light scattering detector (Wyatt Dawn 8) operated with chloroform. The dn/dc value used for PMMA in chloroform was determined to be 0.065 mL/g. The side chain molecular weight was determined by cleaving the side chains from the backbone by methanolysis and characterized using the same GPC procedure as above.[23]

Polymer film samples were prepared by spin coating solutions comprised of 1 wt% polymer solutions in anisole, where the polymer was 0.03:1 dyed to unlabeled polymer by weight. For films used in the solvent swelling experiments, the unlabeled polymer was a 350,000 g/mol linear PMMA. Synthesized bottlebrush polymers were used as the matrices for the bottlebrush

melt samples. All films were prepared on Piranha-treated #1.5 thickness coverslips by spin coating at 800 RPM for 10 seconds and then 3000 RPM for 1 minute to produce 40 nm thick films.

SMLM experiments on polymer films were performed using the same previously reported optical setup.[23,31] This setup features a custom modified Olympus IX73 inverted microscope equipped with optical components from ThorLabs. All super-resolution images were comprised of 10,000 frames taken at 10 ms exposure times. Super-resolution images were analyzed using the imaging processing toolbox in Matlab to trace a central line through relevant features, determining a tangent-tangent correlation function $C(s)$ from these traces, and extracting a persistence length value by the fitting ensemble-average $C(s)$ to an exponential decay. These methods are described in greater detail in earlier work.[23]

Solvent experiments were performed by using a custom-built sample chamber with an inlet for solvent vapor (Figure S1a). The amount of solvent within the system was controlled by two mass flow controllers (MFCs) (Alicat MCS-100SCCM-D/5M). One MFC bubbled nitrogen gas through toluene while the other streamed directly to the chamber at a total flow rate of 100 sccm (Figure S1b-c). The ratio between the two flows allowed for control over the vapor pressure of toluene within the chamber. During *in situ* imaging experiments, the flow rates on the MFCs were kept constant for two hours before imaging at each solvent condition to ensure the sample reached an equilibrium swelling condition. The conditions used ranged from 30-70% of the saturated toluene stream, resulting in swelling ratios between 5-30%. Swelling ratio is defined by the fractional mass increase relative to the original mass of the dry film, given by,

$$Swelling\ Ratio = \frac{W_s - W_i}{W_i} \quad (1)$$

where W_s is the weight of the swollen film and W_i is the weight of the dry film before swelling. The swelling ratio was later confirmed using quartz crystal microbalance (QCM) (Advanced Wave

Sensors, Valencia, Spain) with a N2PK impedance analyzer (Thornhill Canada), equipped with a near-identical solvent setup. More on QCM measurements can be found in Section 3 of the Supporting Information.

Results and Discussion

To study the effects of the local environment on the conformation and behavior of bottlebrush polymers, we devised a set of single-molecule localization microscopy (SMLM) imaging experiments on bottlebrushes within linear matrices swollen with solvent and within materials entirely occupied by bottlebrush polymers. For these studies, we revisit the fluorescently-labeled bottlebrush polymers previously reported and investigated in earlier SMLM studies (Table 1).[23] These polymers were prepared using a grafting-from approach, beginning with a poly (2-(2-bromoisobutyryloxy)ethyl methacrylate) (PBIEM) backbone and polymerizing poly(methyl methacrylate) (PMMA) side chains directly from the backbone. These polymers were prepared such that each backbone BIEM repeat unit is expected to have one side chain. By using the same set of polymers as our previous study, we can make direct comparisons between the originally investigated hybrid system to the solvent-swollen system and the bottlebrush melt system discussed in this work.

Table 1: Molecular Weight of Bottlebrush Polymers

M_{sc} (g/mol)	Fluorescent Labeling*	$Đ_{sc}$	M_{bb}, Theoretical (kg/mol)**
640	Labeled	1.10	1,380
1,100	Labeled	1.31	2,240
2,030	Labeled	1.22	3,980
2,860	Labeled	1.22	5,540

3,500	Labeled	1.27	6,730
750	Unlabeled	1.36	1,580
1,000	Unlabeled	1.23	2,050
2,100	Unlabeled	1.58	4,110
2,700	Unlabeled	1.82	5,230
4,020	Unlabeled	1.23	7,700

*The labeled bottlebrushes in this table were synthesized for a previous study and studied again here. The unlabeled bottlebrushes were synthesized for this study.

**The theoretical molecular weight of the full bottlebrush is used as an approximation for comparison. In actuality, the molecular weight is closer to approximately 90% of this value based on our previous measurements.[23]

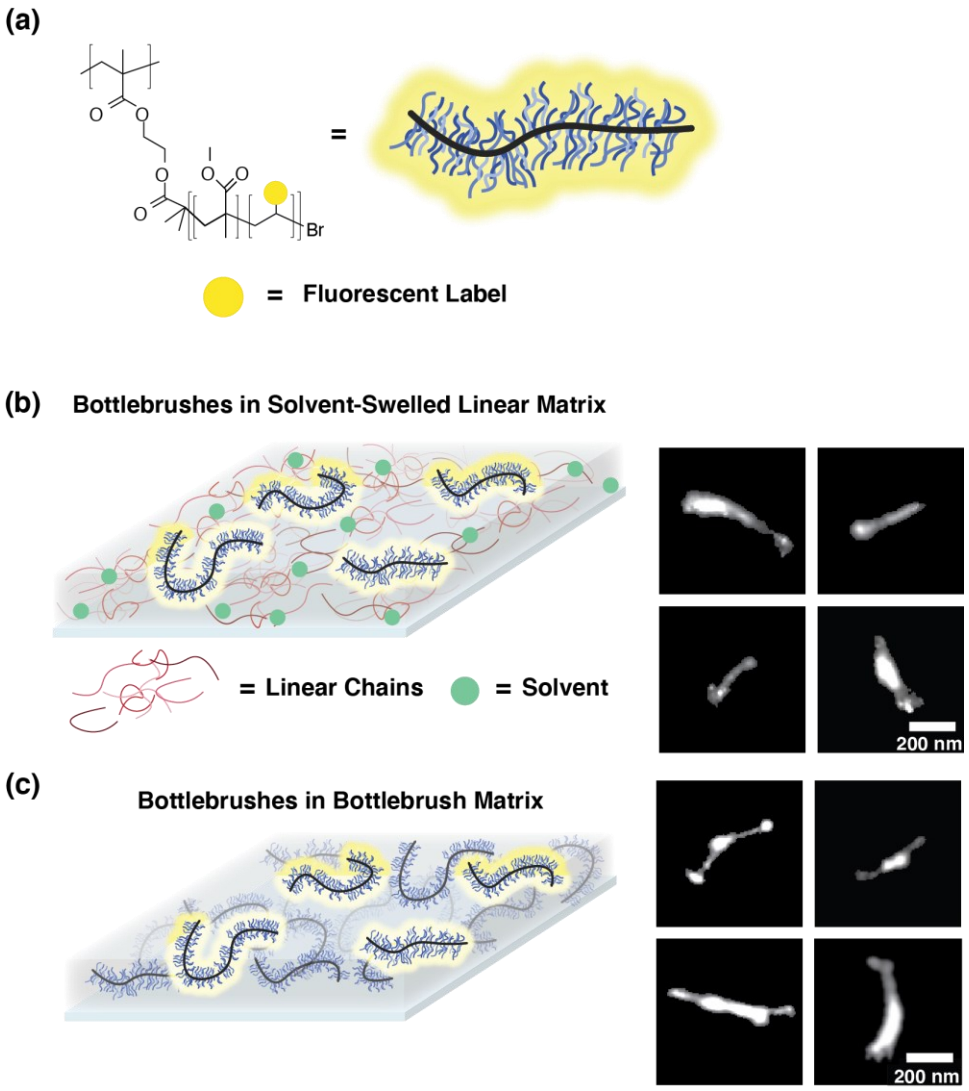

Figure 1: (a) Structure of bottlebrush polymers composed of PMMA side chains and a PBIEM backbone. The fluorescent label is a photoswitchable diarylethene as previously reported.[31,33] (b-c) Schematic and representative features within solvent-swollen linear-bottlebrush hybrid systems and bottlebrush melts. (b) represents a linear matrix swollen with solvent with a dilute amount of labeled bottlebrushes dispersed, and features are single bottlebrush chains (M_{sc} = 3,500 g/mol). (c) represents bottlebrush polymers within a bottlebrush matrix, and features are single bottlebrush chains (M_{sc} = 3,500 g/mol).

In order to test the local environment effects on bottlebrush conformations, we swelled toluene into polymer films comprised of bottlebrushes in a linear matrix. We imaged the five dye-

labeled PMMA bottlebrush polymers with different side chain molecular weights (M_{sc}) in linear matrices comprised of PMMA (350,000 g/mol) (Figure 1) in 40 nm thick polymer films. This thickness is convenient because it is easily within the depth of field of our microscope objective, so 3D conformations can be projected onto 2D images. Additionally, 40 nm is an order of magnitude larger than the expected R_g of the side chains, which should thus be unaffected by confinement effects. Since conformation is driven by the behavior of the side chains, confinement is expected to have negligible effects on the bottlebrushes. In our previous work, we also confirmed that confinement has minimal effect on backbone conformation, using Monte Carlo simulations to show that our established analysis methods can accurately determine a persistence length value from simulated chains in a confined film.[23] Each film was prepared by spin coating and annealed for 2 hours under nitrogen at 180°C. For each of the five bottlebrush conditions, the films were swollen by 70% saturated toluene vapor *in situ* for two hours using a custom sample chamber mounted directly on the microscope (see Supporting Information, Figure S1). resulting in an equilibrium swelling ratio of 0.20. This degree of swelling is not expected to drastically increase the thickness of the sample beyond 20% of the original thickness. The swelling ratio was determined by quartz crystal microbalance (QCM) measured *ex situ* on films in a similar solvent vapor setup (see Supporting Information). Attempting swelling ratios above 0.20 resulted in large fluctuations in the measured mass and were thus unreliable. From these images, we determined an ensemble-averaged persistence length (l_p) for each M_{sc} condition from the tangent-tangent correlation function of the skeletonized trace of the feature. Further details of this analysis are discussed in our previous work.[23] The persistence length results are summarized in Figure 2. We observe a decrease in l_p for each of these bottlebrush conditions for non-swollen to swollen systems. Additionally, we observe a minimal change in the scaling relationship between l_p and M_{sc}.

However, because we have large uncertainties in our determined l_p values, and we only have a few data points that do not span a large range, we hesitate to extract definitive conclusions from these scaling exponents.

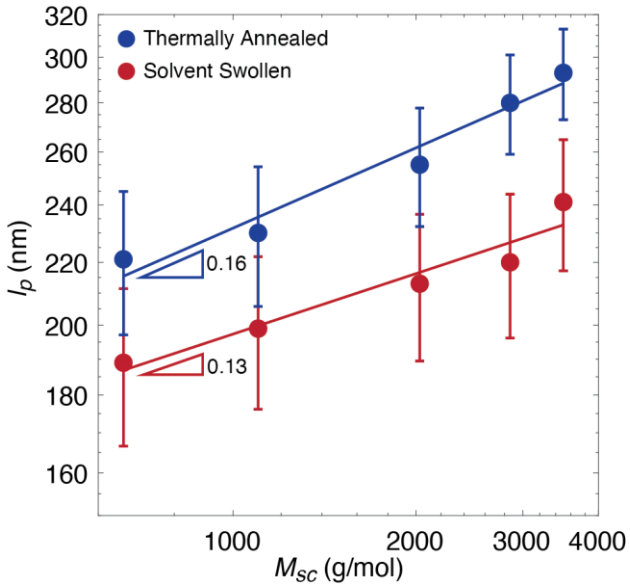

Figure 2: Persistence lengths of PMMA bottlebrush polymers in non-swollen and 20% toluene-swollen linear PMMA films as a function of side chain molecular weight. Each data point consists of 350 chains. Error bars are 90% confidence intervals, which were determined by calculating the standard deviation in l_p based on 10 sets of 350 wormlike chains from simulation (see previous work for details).[22,23] Lines represent power law fits. Due to uncertainties in our technique, we are less confident in lower l_p values. Fitting the highest three points of the solvent-swollen series results in a scaling exponent of 0.22. Note that the data spans less than one decade in the abscissa, so we encourage caution in interpreting the power law fit in general.

To further probe the effects of solvent on bottlebrush conformations within linear matrices, we also explored different swelling ratios under the same M_{sc} condition. Here, we imaged a bottlebrush polymer with M_{sc} of 3,500 g/mol within a linear matrix at swelling ratios of 0-20%

toluene. The lowest swelling condition of 5% was set by the lowest solvent vapor saturation of 30% to produce a mass increase significant from noise. Each condition was held for two hours before imaging to ensure equilibrium conditions. We observed a relatively high persistence length of 290 nm at the no solvent condition, that decreases sharply to 250 nm upon swelling to only 5%. Upon further swelling, the l_p quickly reaches a plateau value of approximately 230 nm. This is rather surprising that only a small amount of solvent in the environment has a large effect on conformation. Perhaps this demonstrates a hard threshold between a highly concentrated regime and neat polymer, where the presence of the solvent at even low concentrations already plays an impact on the physics affecting the system.

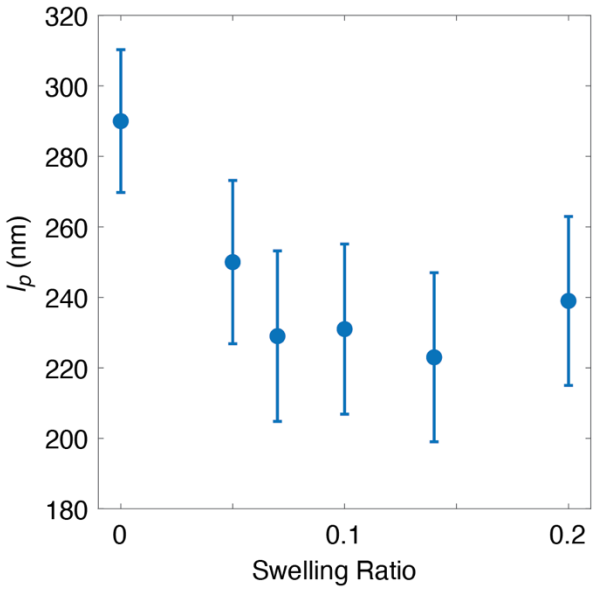

Figure 3: Persistence length of PMMA bottlebrush polymers in linear-bottlebrush hybrid systems at various swelling ratios of toluene (Equation 1). The M_{sc} of the bottlebrush polymer was 3,500 g/mol. Each data point consists of 350 chains. Error bars are the 90% confidence intervals, based on the 10 sets of 350 wormlike chains from simulation.

Based on the difference in the persistence lengths between non-swollen and swollen polymer films, our SMLM experiments suggest that the presence of solvent promotes chain flexibility. This phenomenon can be explained by considering the effects of solvent on the side chains, which largely drive the conformation behavior of the bottlebrush backbone. In our previous work, we hypothesized that autophobic dewetting largely affects the behavior of side chains, which in turn drives the conformation of the entire bottlebrush.[23] Autophobic dewetting occurs in systems with short grafted chains and long matrix chains of the same chemical identity, because it is entropically unfavorable for the matrix chains to interpenetrate into the pervaded volume of the grafted chains.[34] Instead, there are more overall configurations if the grafted chains collapse to a smaller space and the matrix chains occupy the resulting larger separate space. This causes the side chains to behave as hard spheres rather than Gaussian chains, which increases backbone rigidity due to higher degrees of steric repulsion from the bulky groups close to the backbone.

Here, we introduce a good solvent into the local environment surrounding the bottlebrushes, which may relax the side chains from collapsed spheres to swollen coils. This change in behavior drives the overall flexibility of the backbone. The radius of gyration for coils scales as $R_g \sim N^{1/2}$ and for collapsed spheres as $R_g \sim N^{1/3}$, where N is the number of repeat units on the chain and equivalent to M_{sc} here. Based on theory, the persistence length of a bottlebrush in a melt is expected to scale as the size of the side chains $l_p \sim R_g$.[27] However, to our knowledge there is no study in the literature that specifically relates, M_{sc} to l_p under the effect of solvent swelling, and so we propose an explanation for our results here. Although coils are expected to be larger because they are swollen, they are no longer hard spheres and thus their pervaded volumes should easily interpenetrate into each other and with the matrix chains, which decreases steric effects on the backbone and promotes chain flexibility of the entire molecule (Figure 4).

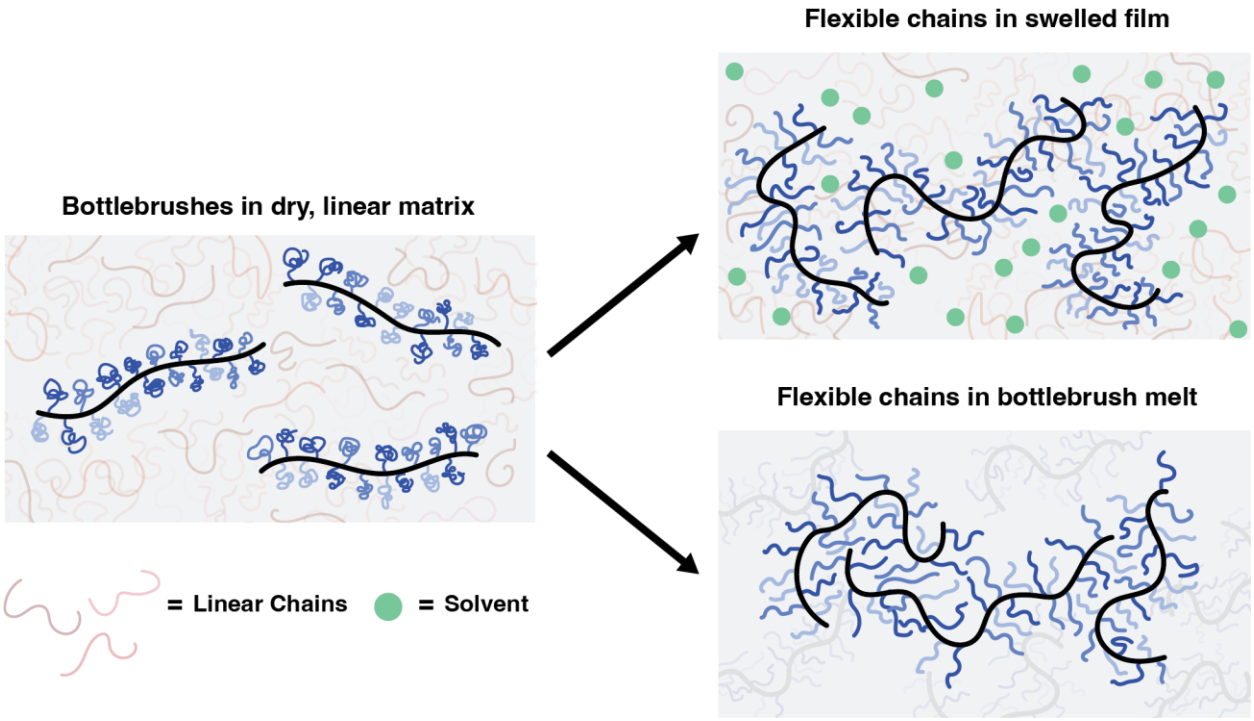

Figure 4: Schematic depicting the effects of autophobic dewetting on bottlebrush conformation. In a dry film comprised of a linear chain matrix, the bottlebrush polymers are rigid due to their collapsed side chains. The addition of solvent relaxes the side chains, and the conformation of the bottlebrushes become more flexible. In a bottlebrush melt, where no autophobic dewetting effects occur, the side chains outstretch, penetrating the pervaded volumes of neighboring chains, allowing them to conform around one another.

Although this proposed mechanism offers a simple explanation for the change in persistence length with respect to solvent swelling, it does not explain the change in the scaling relationship between l_p and M_{sc}. Because we expect the behavior of the entire bottlebrush chain to be driven by the behavior of the side chains as previously hypothesized,[27] we would expect a change in the scaling behavior in addition to the change in rigidity discussed previously. However, we do not observe a significant change in the scaling exponent. While we are cautious to make conclusions on the scaling behavior due to the large uncertainties for l_p values, and the limited less-than-one-decade range over which our data spans, one would expect some variation to reflect

the change in environment. The failure to observe this variation may be an artifact because we are close to the resolution limit of our SMLM imaging technique. As discussed in our previous study, super-resolution microscopy has an implicit resolution limit that affects the accuracy of localizing the fluorescent labels on the bottlebrush. This introduces an uncertainty in fitting the bottlebrush images and extracting an accurate l_p value. From our analysis, we found that this accuracy decreases for l_p values below 200 nm.[23] Therefore, the persistence lengths determined for the lower M_{sc} conditions are less reliable, and this may explain the discrepancy when comparing our results to the theoretically expected scaling relationship. Because our analysis tool often overestimates l_p under these conditions, a higher scaling exponent could be expected without this resolution limit. Excluding the lowest two points leads to a scaling exponent of 0.22. However, because of the inherent uncertainties, it is difficult to make a strong assertion from this result. Nevertheless, we do observe a consistent and reliable decrease in persistence length for many of the M_{sc} condition, so we assert that solvent has some effect promoting chain flexibility.

Despite being close to the resolution limit of our technique and facing difficulty resolving the entire contour of the bottlebrush chains, we do observe a qualitative difference in the features between non-swollen and swollen films (Figure 5a). For conditions with shorter side chains (M_{sc} = 640 and 1,100 g/mol), we observe many more features that are coiled and fewer that are rod-like than we would typically expect. These features are much larger than artifacts that arise from fluorescent impurities, which are generally less than 100 nm in size. Because of this, we suspect we are observing the effects of solvent increasing chain flexibility to such a degree where they no longer appear elongated. We test this theory by studying the aspect ratio of the features found in these swelling experiments. Here, we define an aspect ratio as a ratio between the major and minor axes of an ellipse fit to the feature (Figure 5b), derived from the eigenvalues of the covariance

matrix of the positions of the fluorophore localization events in the SMLM experiment. From this ratio, we can quantify the shape of each feature, where a lower value indicates a more coiled conformation and a higher value indicates a more rod-like conformation. Prior to swelling with solvent, we observe a greater population of higher aspect ratio features (Figure 5c). Additionally, we compared two different M_{sc} conditions (M_{sc} = 640 and 3,500) swollen with toluene at a 20% swelling ratio, which shows this aspect ratio also decreases with M_{sc}. Therefore, these results suggest that for lower M_{sc} conditions only, the solvent induces flexibility to such an extent that their entire contour is no longer visible with the resolution capabilities of SMLM. As we reach this limit, we can no longer reliably determine the persistence lengths, resulting in large uncertainties and scaling relationships that deviate significantly from theory. Although the resolution limits of our technique result in these uncertainties, the aspect ratio analysis provides additional confidence that solvent swelling indeed increases backbone flexibility, consistent with the mechanism of reduced autophobic dewetting.

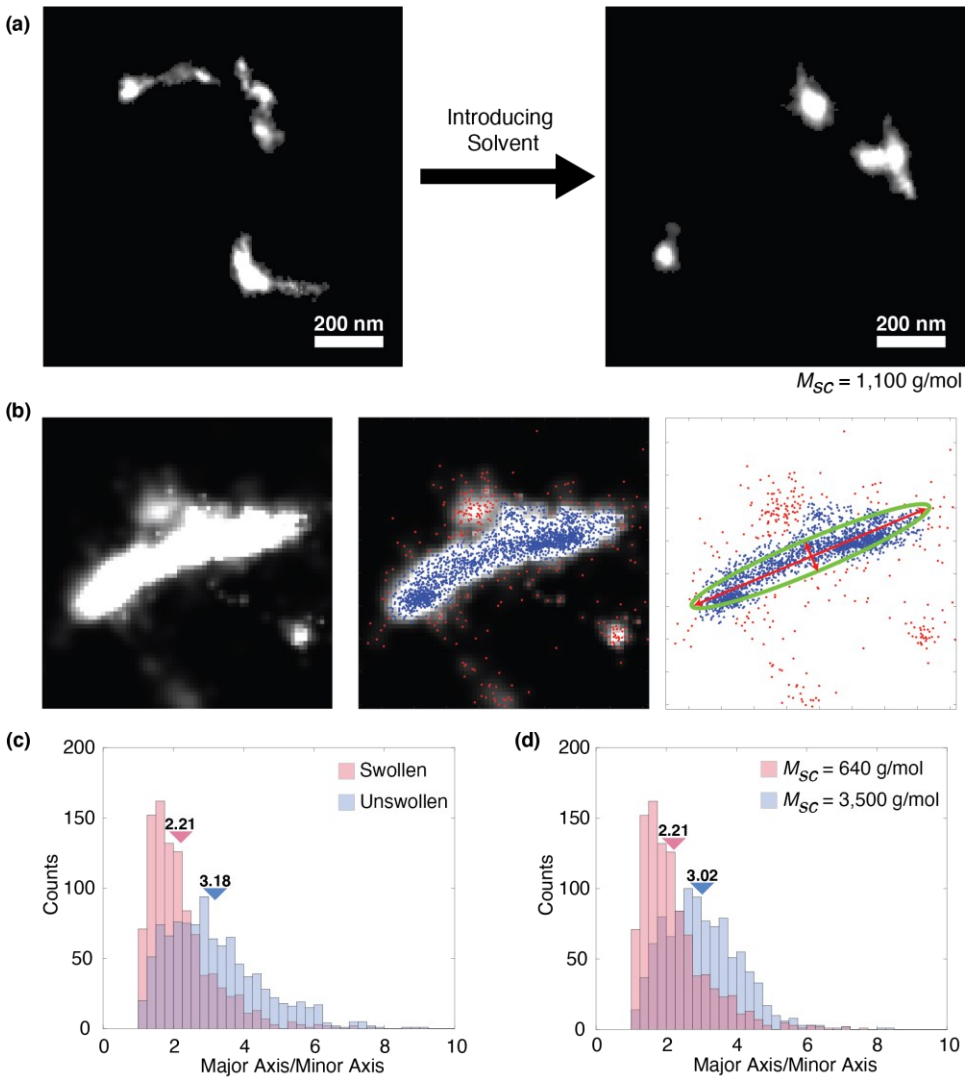

Figure 5: (a) Representative data showing solvent effects on low M_{sc} conditions. Bottlebrushes here have M_{sc} = 1,100 g/mol. The two images show different regions within the same sample before and after swelling with solvent, but they do not reflect the same bottlebrushes. (b) Schematic determining major and minor axes from super-resolution images. (From left to right) The first panel shows the super-resolution image of a single bottlebrush feature. The second panel is the same image with the localizations superimposed on top. The blue dots represent localizations that fall within the pixels belonging to the bottlebrush feature, which is determined by our analysis procedure. Red dots are localizations that fall outside of this feature. This process is described in more detail in our previous work.[23] The third panel displays only the localizations with the fitted ellipse plotted over the points. The red arrows represent the major and minor axes of the ellipse. (c) Histogram of aspect ratios from swollen (at 20% swelling ratio) and unswollen sample. These data reflect the same sample, where M_{sc} = 640 g/mol. Each condition consists of 1,000 features. Triangles indicate the

mean of each condition (2.21 for swollen, 3.18 for unswollen) (d) Histogram of aspect ratios of two different swollen samples with different side chain lengths. Both conditions are swollen at 20% swelling ratio. Each condition consists of 1,000 features. Triangles indicate the mean of each condition (2.21 for 640 g/mol, 3.02 for unswollen 3,500 g/mol).

While ideally an even more powerful experiment would track the exact same chains under different solvent swelling conditions, we do not currently have the technical capabilities to perform such experiments. One of the challenges that limits our abilities is the lifetime of the dye under photobleaching conditions. Currently, it is difficult to perform long time-lapse experiments because as dyes photobleach, the quality of the resulting super-resolution image drops. Additionally, chains are expected to migrate and change in conformation as a result of solvent swelling. Compounded with sample drift and photobleaching, this makes it difficult to ensure that features observed early in acquisition are the same features later into an *in situ* experiment. We therefore rely on analyses that average over a large ensemble to make conclusions on effects of solvent swelling.

To further explore the effect of the surrounding environment on bottlebrush conformations, we study systems where the matrix is entirely composed of bottlebrushes. In these systems, autophobic dewetting is not expected to occur at all because there are no large molecular weight differences between side chains of neighboring bottlebrushes. We synthesized five different bottlebrush polymers containing no fluorescent labels for the matrix of these samples, each matching one of the five dye-labeled bottlebrush polymers previously used (Table 1). Each labeled system was blended with their corresponding unlabeled matrix and persistence lengths were extracted using the same methods as previously discussed (Figure 6). The persistence lengths decreased for each of the melt systems compared to those previously reported for linear matrices. Additionally, the l_p vs. M_{sc} scaling exponent appears to increase from 0.16 to 0.39, though we

caution the reader about overinterpretation similarly to above, due to the relatively large uncertainties and small span of the data.

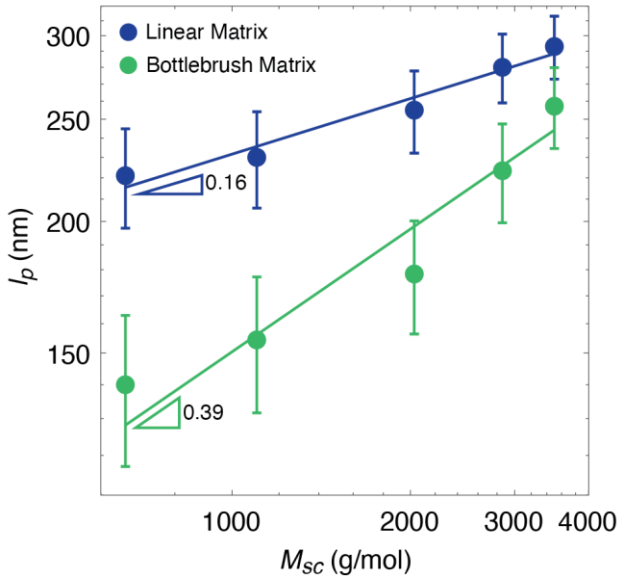

Figure 6: Persistence lengths of bottlebrush polymers in linear and bottlebrush matrices with respect to side chain molecular weight. The linear matrix data is identical to Figure 2. Each data point is based 350 chains. Error bars are the 90% confidence intervals, based on 10 sets of 350 simulated wormlike chains. Lines represent a power law fit. Due to uncertainties in our technique, we are less confident in lower l_p values. Fitting the highest four points of the bottlebrush matrix series results in a scaling exponent of 0.47. Note that the data spans less than one decade in the abscissa, so we encourage caution in interpreting the power law fit in general.

When transitioning from a linear to a bottlebrush matrix, the decrease in persistence lengths and increase in l_p vs. M_{sc} scaling are consistent with the removal of autophobic dewetting effects. In a matrix comprised of bottlebrushes rather than linear polymers, there is no large molecular weight mismatch, and the number of configurations is not reduced when the side chains

interpenetrate with those of neighboring bottlebrushes (Figure 4). Therefore, there is no entropic penalty for the side chains to behave as Gaussian chains, leading to much greater backbone flexibility. This is reflected in our extracted l_p values, where we observe a decrease for each of the M_{sc} conditions. Additionally, the scaling exponent of 0.39 is closer to the expected value of 0.5 for bottlebrush melts, which has been reported in various theoretical studies.[27–29] As previously discussed, because of the resolution limitations in our super-resolution imaging and analysis tool, the lower extracted persistence length values at the lowest M_{sc} conditions are potentially overestimations of the true value. Eliminating the lowest data point leads to a scaling exponent of 0.47. However, because we are near this resolution limit, we are cautious to extract definitive conclusions on the scaling behavior. The overall trends observed here do provide some evidence that bottlebrushes within a bottlebrush matrix deviate from those within a linear matrix, where autophobic dewetting effects may largely drive behavior. Overall, the increased flexibility and scaling behavior observed through these SMLM experiments is consistent with explanations proposed for our previous work and with theoretical studies on bottlebrush melts.

Conclusion

In this work, we expanded on our previous investigations using SMLM to study single chain conformations of bottlebrush polymers to understand the effect on chain rigidity from changes to local environments around the bottlebrush. From our previous experiments, we hypothesized that autophobic dewetting in linear-bottlebrush hybrid systems caused highly rigid bottlebrushes that diverged greatly from expected behaviors based in theory. Here, we introduced conditions that opposed these entropic effects and reduced autophobic dewetting. Although we observed more flexible chains within these solvent-swollen systems, the expected scaling behavior

between l_p and M_{sc} did not precisely follow our expectations, which may be due to the resolution limit of our imaging technique. We additionally investigated neat systems entirely comprised of bottlebrush polymers. Here, we also observed greater flexibility and a scaling relationship closer to theoretical predictions. Despite working close to the SMLM resolution limit, our results indicate a change in the scaling relationship that more closely resembles theoretical studies on similar systems. Overall, expanding on our SMLM experiments provides evidence that local environment plays a large role on chain conformation, further supporting our previous theories that autophobic dewetting significantly affects bottlebrush rigidity.

Acknowledgments

The authors acknowledge Profs. Julia Kalow, and John Torkelson for access to equipment and useful discussions, and funding from the National Science Foundation (DMR-1945249) for support of this work. M.W. acknowledges support from the Alfred P. Sloan Foundation and The Camille and Henry Dreyfus Foundation. This work made use of the Integrated Molecular Structure Education and Research Center (IMSERC) facility at Northwestern University, which has received support from the Soft and Hybrid Nanotechnology Experimental Resource (NSF ECCS-2025633), the State of Illinois, and the International Institute for Nanotechnology.

References

(1) Yin, X.; Qiao, Y.; Gadinski, M. R.; Wang, Q.; Tang, C. Flexible Thiophene Polymers: A Concerted Macromolecular Architecture for Dielectrics. *Polym Chem* **2016**, *7* (17), 2929–2933. https://doi.org/10.1039/c6py00233a.

(2) Tonge, C. M.; Sauvé, E. R.; Cheng, S.; Howard, T. A.; Hudson, Z. M. Multiblock Bottlebrush Nanofibers from Organic Electronic Materials. *J Am Chem Soc* **2018**, *140* (37), 11599–11603. https://doi.org/10.1021/jacs.8b07915.

(3) Vatankhah-Varnosfaderani, M.; Keith, A. N.; Cong, Y.; Liang, H.; Rosenthal, M.; Sztucki, M.; Clair, C.; Magonov, S.; Ivanov, D. A.; Dobrynin, A. V.; Sheiko, S. S. Chameleon-like Elastomers with Molecularly Encoded Strain-Adaptive Stiffening and Coloration. *Science (1979)* **2018**, *359* (6383), 1509–1513. https://doi.org/10.1126/science.aar5308.

(4) Keith, A. N.; Vatankhah-Varnosfaderani, M.; Clair, C.; Fahimipour, F.; Dashtimoghadam, E.; Lallam, A.; Sztucki, M.; Ivanov, D. A.; Liang, H.; Dobrynin, A. V.; Sheiko, S. S. Bottlebrush Bridge between Soft Gels and Firm Tissues. *ACS Cent Sci* **2020**, *6* (3), 413–419. https://doi.org/10.1021/acscentsci.9b01216.

(5) Daniel, W. F. M.; Burdyńska, J.; Vatankhah-Varnoosfaderani, M.; Matyjaszewski, K.; Paturej, J.; Rubinstein, M.; Dobrynin, A. V.; Sheiko, S. S. Solvent-Free, Supersoft and Superelastic Bottlebrush Melts and Networks. *Nat Mater* **2016**, *15* (2), 183–189. https://doi.org/10.1038/nmat4508.

(6) Vatankhah-Varnosfaderani, M.; Daniel, W. F. M.; Everhart, M. H.; Pandya, A. A.; Liang, H.; Matyjaszewski, K.; Dobrynin, A. V.; Sheiko, S. S. Mimicking Biological Stress-Strain Behaviour with Synthetic Elastomers. *Nature* **2017**, *549* (7673), 497–501. https://doi.org/10.1038/nature23673.

(7) Patel, B. B.; Walsh, D. J.; Kim, D. H.; Kwok, J.; Lee, B.; Guironnet, D.; Diao, Y. Tunable Structural Color of Bottlebrush Block Copolymers through Direct-Write 3D Printing from Solution. *Sci Adv* **2020**, *6* (24), eaaz7202, 1–13. https://doi.org/10.1126/sciadv.aaz7202.

(8) Xie, R.; Mukherjee, S.; Levi, A. E.; Reynolds, V. G.; Wang, H.; Chabinyc, M. L.; Bates, C. M. Room Temperature 3D Printing of Super-Soft and Solvent-Free Elastomers. *Sci Adv* **2020**, *6* (46), 1–11. https://doi.org/10.1126/sciadv.abc6900.

(9) Self, J. L.; Sample, C. S.; Levi, A. E.; Li, K.; Xie, R.; De Alaniz, J. R.; Bates, C. M. Dynamic Bottlebrush Polymer Networks: Self-Healing in Super-Soft Materials. *J Am Chem Soc* **2020**, *142* (16), 7567–7573. https://doi.org/10.1021/jacs.0c01467.

(10) Sunday, D. F.; Chremos, A.; Martin, T. B.; Chang, A. B.; Burns, A. B.; Grubbs, R. H. Concentration Dependence of the Size and Symmetry of a Bottlebrush Polymer in a Good Solvent. *Macromolecules* **2020**, *53* (16), 7132–7140. https://doi.org/10.1021/acs.macromol.0c01181.

(11) López-Barrón, C. R.; Shivokhin, M. E. Extensional Strain Hardening in Highly Entangled Molecular Bottlebrushes. *Phys Rev Lett* **2019**, *122* (3), 37801. https://doi.org/10.1103/PhysRevLett.122.037801.

(12) López-Barrón, C. R.; Tsou, A. H.; Hagadorn, J. R.; Throckmorton, J. A. Highly Entangled α - Ole Fi n Molecular Bottlebrushes: Melt Structure, Linear Rheology, and Interchain Friction Mechanisḿ. **2018**. https://doi.org/10.1021/acs.macromol.8b01431.

(13) Dalsin, S. J.; Hillmyer, M. A.; Bates, F. S. Linear Rheology of Polyolefin-Based Bottlebrush Polymers. *Macromolecules* **2015**, *48* (13), 4680–4691. https://doi.org/10.1021/acs.macromol.5b01153.

(14) Haugan, I. N.; Maher, M. J.; Chang, A. B.; Lin, T. P.; Grubbs, R. H.; Hillmyer, M. A.; Bates, F. S. Consequences of Grafting Density on the Linear Viscoelastic Behavior of Graft Polymers. *ACS Macro Lett* **2018**, *7* (5), 525–530. https://doi.org/10.1021/acsmacrolett.8b00116.

(15) Pesek, S. L.; Li, X.; Hammouda, B.; Hong, K.; Verduzco, R. Small-Angle Neutron Scattering Analysis of Bottlebrush Polymers Prepared via Grafting-through

Polymerization. *Macromolecules* **2013**, *46* (17), 6998–7005. https://doi.org/10.1021/ma401246b.
(16) Pesek, S. L.; Xiang, Q.; Hammouda, B.; Verduzco, R. Small-Angle Neutron Scattering Analysis of Bottlebrush Backbone and Side Chain Flexibility. *J Polym Sci B Polym Phys* **2017**, *55* (1), 104–111. https://doi.org/10.1002/polb.24251.
(17) Sunday, D. F.; Chang, A. B.; Liman, C. D.; Gann, E.; Delongchamp, D. M.; Thomsen, L.; Matsen, M. W.; Grubbs, R. H.; Soles, C. L. Self-Assembly of ABC Bottlebrush Triblock Terpolymers with Evidence for Looped Backbone Conformations. *Macromolecules* **2018**, *51* (18), 7178–7185. https://doi.org/10.1021/acs.macromol.8b01370.
(18) Dalsin, S. J.; Rions-Maehren, T. G.; Beam, M. D.; Bates, F. S.; Hillmyer, M. A.; Matsen, M. W. Bottlebrush Block Polmers: Quantitative Theory and Experiments. *ACS Nano* **2015**, *9* (12), 12233–12245. https://doi.org/10.1021/acsnano.5b05473.
(19) Borodinov, N.; Belianinov, A.; Chang, D.; Carrillo, J. M.; Burch, M. J.; Xu, Y.; Hong, K.; Ievlev, A. V.; Sumpter, B. G.; Ovchinnikova, O. S. Molecular Reorganization in Bulk Bottlebrush Polymers: Direct Observation: Via Nanoscale Imaging. *Nanoscale* **2018**, *10* (37), 18001–18009. https://doi.org/10.1039/c8nr05630g.
(20) Thompson, M. A.; Lew, M. D.; Moerner, W. E. Extending Microscopic Resolution with Single-Molecule Imaging and Active Control. *Annu Rev Biophys* **2012**, *41* (1), 321–342. https://doi.org/10.1146/annurev-biophys-050511-102250.
(21) Qiang, Z.; Wang, M. 100th Anniversary of Macromolecular Science Viewpoint: Enabling Advances in Fluorescence Microscopy Techniques. *ACS Macro Lett* **2020**, *9* (9), 1342–1356. https://doi.org/10.1021/acsmacrolett.0c00506.
(22) Chan, J. M.; Wang, M. Visualizing the Orientation of Single Polymers Induced by Spin-Coating. *Nano Lett* **2022**. https://doi.org/10.1021/acs.nanolett.2c01830.
(23) Chan, J. M.; Kordon, A. C.; Zhang, R.; Wang, M. Direct Visualization of Bottlebrush Polymer Conformations in the Solid State. *Proc Natl Acad Sci U S A* **2021**, *118* (40), 1–9. https://doi.org/10.1073/pnas.2109534118.
(24) Sveinbjornsson, B. R.; Weitekamp, R. A.; Miyake, G. M.; Xia, Y.; Atwater, H. A.; Grubbs, R. H. Rapid Self-Assembly of Brush Block Copolymers to Photonic Crystals. *Proceedings of the National Academy of Sciences* **2012**, *109* (36), 14332–14336. https://doi.org/10.1073/pnas.1213055109.
(25) Song, D. P.; Zhao, T. H.; Guidetti, G.; Vignolini, S.; Parker, R. M. Hierarchical Photonic Pigments via the Confined Self-Assembly of Bottlebrush Block Copolymers. *ACS Nano* **2019**, *13* (2), 1764–1771. https://doi.org/10.1021/acsnano.8b07845.
(26) Daniel, W. F. M.; Burdyńska, J.; Vatankhah-Varnoosfaderani, M.; Matyjaszewski, K.; Paturej, J.; Rubinstein, M.; Dobrynin, A. V.; Sheiko, S. S. Solvent-Free, Supersoft and Superelastic Bottlebrush Melts and Networks. *Nat Mater* **2016**, *15* (2), 183–189. https://doi.org/10.1038/nmat4508.
(27) Paturej, J.; Sheiko, S. S.; Panyukov, S.; Rubinstein, M. Molecular Structure of Bottlebrush Polymers in Melts. *Sci Adv* **2016**, *2* (11). https://doi.org/10.1126/sciadv.1601478.
(28) Liang, H.; Cao, Z.; Wang, Z.; Sheiko, S. S.; Dobrynin, A. V. Combs and Bottlebrushes in a Melt. *Macromolecules* **2017**, *50* (8), 3430–3437. https://doi.org/10.1021/acs.macromol.7b00364.
(29) Liang, H.; Wang, Z.; Sheiko, S. S.; Dobrynin, A. V. Comb and Bottlebrush Graft Copolymers in a Melt. *Macromolecules* **2019**, *52* (10), 3942–3950. https://doi.org/10.1021/acs.macromol.9b00611.

(30) Rzayev, J. Synthesis of Polystyrene-Polylactide Bottlebrush Block Copolymers and Their Melt Self-Assembly into Large Domain Nanostructures. *Macromolecules* **2009**, *42* (6), 2135–2141. https://doi.org/10.1021/ma802304y.
(31) Qiang, Z.; Shebek, K. M.; Irie, M.; Wang, M. A Polymerizable Photoswitchable Fluorophore for Super-Resolution Imaging of Polymer Self-Assembly and Dynamics. *ACS Macro Lett* **2018**, *7* (12), 1432–1437. https://doi.org/10.1021/acsmacrolett.8b00686.
(32) Uno, K.; Niikura, H.; Morimoto, M.; Ishibashi, Y.; Miyasaka, H.; Irie, M. In Situ Preparation of Highly Fluorescent Dyes upon Photoirradiation. *J Am Chem Soc* **2011**, *133* (34), 13558–13564. https://doi.org/10.1021/ja204583e.
(33) Uno, K.; Niikura, H.; Morimoto, M.; Ishibashi, Y.; Miyasaka, H.; Irie, M. In Situ Preparation of Highly Fluorescent Dyes upon Photoirradiation. *J Am Chem Soc* **2011**, *133* (34), 13558–13564. https://doi.org/10.1021/ja204583e.
(34) Green, P. F. The Structure of Chain End-Grafted Nanoparticle/Homopolymer Nanocomposites. *Soft Matter* **2011**, *7* (18), 7914–7926. https://doi.org/10.1039/c1sm05076a.